ISSN 2303-4521
Periodicals of Engineering and Natural Sciences *Original Research*
Vol. 10, No. 2, April 2022, pp.512-538

Numerical modeling of the experimental test for shear strengthened of fire damaged high strength lightweight RC beams with SIFCON jacket

Ahmed Habeeb Albo Sabar[1], Mohammed Mansour Kadhum[2]
[1] Civil Engineering Department, College of Engineering, University of Babylon, Babylon, Iraq
[2] College of Engineering, University of Babylon, Babylon, Iraq

ABSTRACT

The behaviour of concrete structures when exposed to fire is essential because fire represents an excessive loading and critical structural case for any concrete structure. This paper discusses the adopted procedure for modelling and simulation of concrete beams that experimentally tested in the lab. Through using of ABAQUS program, a finite model of lightweight reinforced concrete beams was carried out under realistic fire circumstances. 14 Beam specimens with lightweight high strength types, before and after firing up to 600°C, and improvement with SIFCON jacketing technique, were simulated and compared with the experimental results. For both the displacement at mid span and the maximum load carrying capacity of the specimens, the absolute error between experimental and numerical values was determined. From the results, it can be seen that the minimum and maximum determined absolute error for specimens' load carrying capacity was about 0.521% and 15.61%, respectively. on the other side, minimum and maximum determined absolute error for specimens' displacement corresponded to the max load were 0.42% and 11.42%, respectively. accordingly, and since the estimated errors less than 15%, it can be said that the performed simulation process was accurate and successful when compared with other researchers' studies. As a result, it was found that there is an agreement between the practical and theoretical findings of the study, and a helpful tool for predicting failure in the event of a fire occurrence is provided.

Keywords: Finite Element Modelling,Abaqus , SIFCON, Fire Damage, High Strength Concrete

Corresponding Author:

Ahmed Habeeb Albo Sabar
Civil Engineering Department
University of Babylon, Iraq
ahmed.youssef@student.uobabylon.edu.iq

1. Introduction

Concrete buildings have excellent fire resistance and can have a very high residual strength, and it can offer some thermal protection for steel reinforcement due to its poor thermal conductivity, delayed strength deterioration at high temperatures, and high heat capacity [1–3The fire safety of structural members is measured in terms of duration in terms of structural stability and integrity [4, 5], that is, the behavior of concrete members subjected to temperature–time curves as given by ASTM E119 [6], EN 1992–1-2 [7], ISO 834–1 [8], and BS 476–20 [9].In most circumstances, concrete could be re-used based on the condition of a building after a fire, the remaining load capacity, acceptable remaining displacements, and the load usage level. As a result, resistance to fire of high strength lightweight RC members is becoming a significant characteristic in present design codes such as Eurocode2 [7], and ACI 216.1 [1].

During a fire, the concrete is subjected to a highly higher temperature, which causes a significant reduction in concrete characteristics such as compressive strength and ductility, especially at temperatures above 550oC. The binding materials begin to disintegrate at higher temperatures (700oC or higher), resulting in a significant loss of reinforced concrete mechanical properties (stiffness and compressive strength) (RC). Moreover, the

concrete suffers from the weakening of the aggregate-cement paste bonds, which resulting of cracking and a dramatic deterioration of the concrete's lay. As a result, the structural components' capacities cannot bear both dead and living loads unless they are reinforced [10,11].

For normal strength concrete (NSC) at high temperatures, several models have been described for compressive strength, tensile strength, elastic modulus, peak strain, and stress–strain relations, but only a few models for high strength concrete (HSC) under burning exist. In the building and construction industry, HSC is becoming more popular; nonetheless, HSC reacts differently under fire than NSC. HSC is more prone to spalling and loses compressive strength and elastic modulus at a faster rate than NSC [12]. As a result, it is essential that these features be properly represented for numerical analysis.

Nowadays, the performance-based fire safety design technique has steadily become the preferred way [13], resulting in numerical modeling of reinforced concrete members at high temperature [14, 15]. Various numerical models were developed to simulate heat flow, structural, and thermal performance of concrete parts or structures [16–19]. Finite Elements is the most often utilized approach in recent studies [20–23]. Despite the fact that the structural and thermal behavior of concrete at room temperature is well documented, data on the structural and thermal behavior of concrete at higher temperatures is few.

Design codes have been created to provide reliable guidance for the design and analysis of concrete structures exposed to fire. They present simpler formulas derived experimentally from experimental data gathered during a standardized fire test [24].

2. Experimental work

An experimental test was done to understand the structural behavior of lightweight concrete beams exposed to fire to get a knowledge of the thermal effects on reinforced concrete structural members. As a result, the following goals were examined:

1- To investigate the reaction of lightweight concrete before and after fire exposure.
2- To evaluate the reduction of shear strength and load carrying capacity associated with varying periods of fire exposure.
3- Examine the shear performance and failure mechanism of simply supported beams with SIFCON jackets externally reinforced.
4- comparing the behaviour, mode of cracking, and failure of reinforced concrete beams before and after strengthening with SIFCON jacket, with respect to the resistance to applied shear stresses.

2.1 Properties of materials

Ordinary Portland cement was employed in this investigation. It was made in Iraq and marketed in local markets under the trademark (Karasta). The primary concrete mixture included natural sand from a local resource donated by Kerbala as a fine aggregate. The sand used in the SIFCON slurry must be thin enough to penetrate the thick steel fiber completely without clogging. The only fine sand that was sieved through (1.18 mm sieve) to filter out the coarser particles during the trial work for all SIFCON mixes can be used in the SIFCON slurry formation.

The expanded clay aggregate (LECA) was chosen, and it was imported from north of Tehran City, Iran, with uniform sizes ranging from 0.475 cm to 1 cm. Porous ceramic elements with uniform, small, closed-cell pores, as well as strongly sintered and robust external surfaces, make up this type of lightweight aggregate. LECA is manufactured from raw clay mineral sources that are burned in rotary kilns at temperatures between 1100 and 1200° C, resulting in considerable particle volume swelling.

In this study, silica fume, also known as Mega Add MS (D) from CONMIX, was utilized to replace approximately 10% of the cement in both high strength lightweight concrete and SIFCON mixes. Silica fume enhances the microstructure of cement paste, making it more resistant to external influences.

The reinforcing material is a slurry with a maximum aggregate size of 1.18 mm and a water/binder (cement + micro silica) ratio of 0.33. Hooked end steel fibers with 30mm length, 0.5mm diameter, L/D ratio of 60, and tensile strength of 1100 MPa. are used to strengthen the mortar at a rate of 6 percent (by volume). Figures (1) and (2) show the chosen mixtures after several trial mixes for HSLWC and SIFCON, respectively.

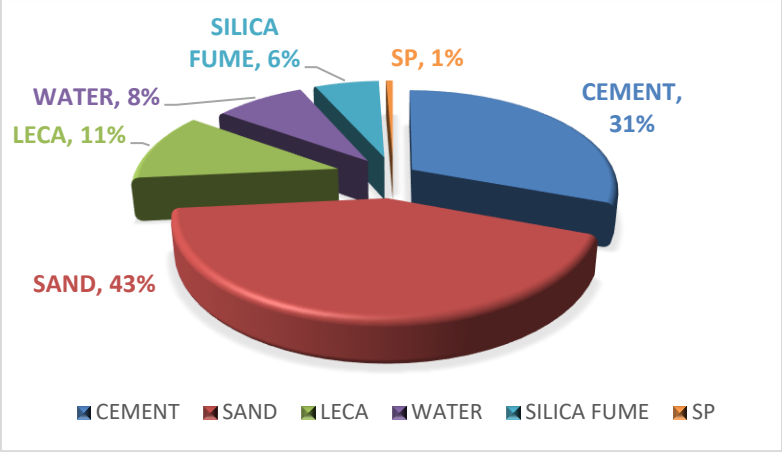

Figure 1. The percentage of materials utilized in the HSLWC mixture (percent of total mix weight)

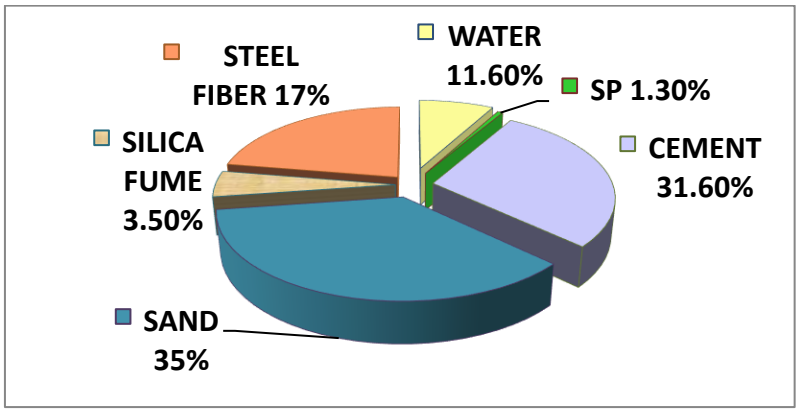

Figure 2. SIFCON combination material percentage (percent of total mix weight)

2.2 Specimens manufacture and testing setup

As indicated in Figure (3), testing was carried out on fourteen 2000 mm long beams having a depth of 200 mm and a width of 150 mm. Three bottoms longitudinal rebars (Ø= 12 mm), two tops longitudinal rebars (Ø= 10 mm), and stirrups with a diameter of 8 mm and a spacing of 200 mm were used to strengthen the beams. The bottom longitudinal rebars ends were hooked to ensure a good anchoring and to prevent sliding under loading.

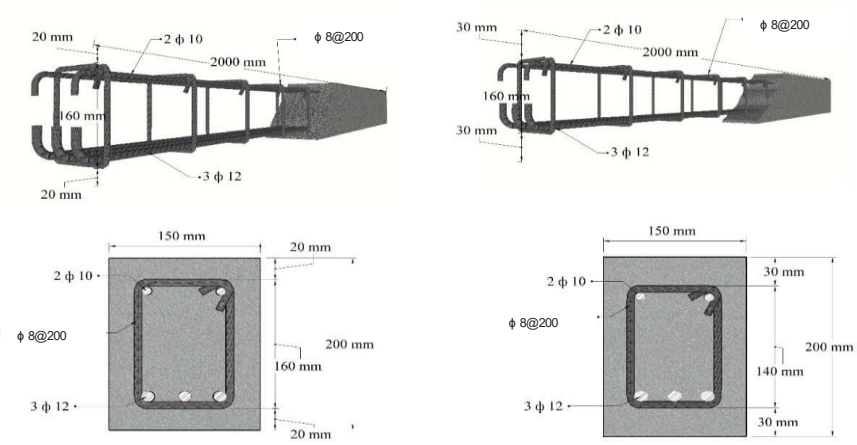

Figure 3. LWC beam cross-section geometry

These beam specimens divided into two main groups, first group including the beams with concrete cover of 20mm and the second group including these were made with 30mm concrete cover. Each one of these groups dividing into four subcategories, the first included beams that were exposed to fire and were not strengthened, the second included the beams that were exposed to fire and were strengthened using SIFCON jacket with thickness of 20mm., the third subcategory included beams that were exposed to fire and were strengthened using a jacket with a thickness of 30mm. The fourth subcategory included beams that were not exposed to fire and were not strengthened with SIFCON, which was used as a control for tested beams. Each of the four subcategories was divided based on the duration of exposure. The main goal is to select the best cover and SIFCON jacket thickness to reduce the deterioration and spalling effects of the original lightweight concrete beam exposed to fire flame, as well as to meet the practical requirements for load carrying capacity and energy absorption, as well as to eliminate brittle shear failure and increase the ultimate shear strength of the repaired beams by using SIFCON jackets as external shear reinforcements. As indicated in Figure (4), a two-point flexural loading mechanism is used.

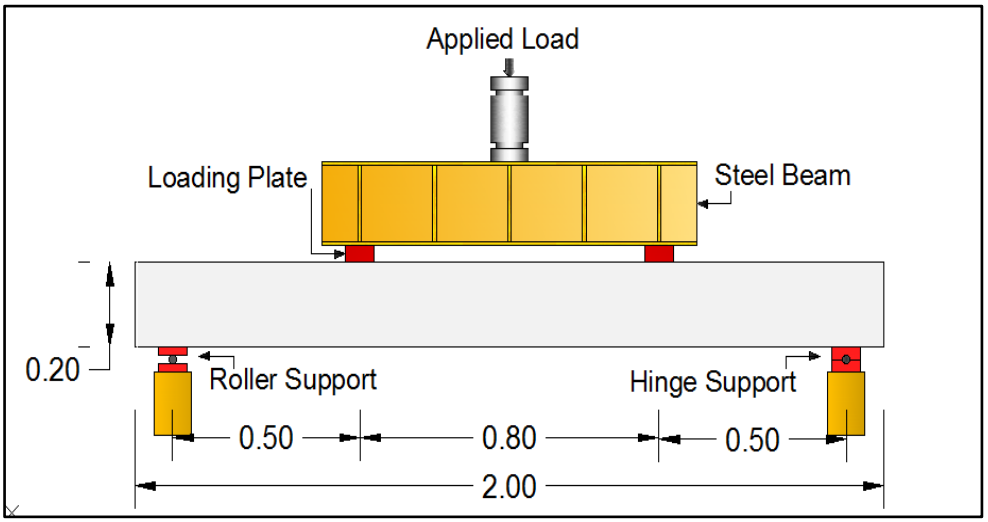

Figure 4. The mechanical loading configurations

At each stage of loading, three LVDTs instrument were used to measure the displacement of the beam at the mid-span of the specimen and under the location of the two-point loading.

Two LVDTs are installed along the top and bottom faces of the beam to monitor changes in displacements across a distance of 20 cm, which is used to determine the mid-span curvature of the beam, as shown in figure (9). The load was applied in small increments until the failure.

2.3 Techniques Used in Loading fire.

A special brick furnace was made locally and equipped with thermocouple sensors and portable data collection devices to record the temperature change over time, used to expose the constructed concrete beams to fire conditions, as shown in Figure (6). The HSLWC beams were placed in the oven and subjected to fire after age of 56 days. In the oven, the beams were burnt in accordance with ISO-834 fire standard.

The furnace was built to withstand temperatures up to 1200 degrees Celsius. The furnace temperature was set to follow the ISO curve. After the burning process and complete cooling of the beam specimen to ambient temperature (about 35 °C), extensive crack and spalling intensity measurements were performed. The real temperature-time curve was constructed with the Matlab application, that connected the thermocouple in the furnace to the computer and allowed temperature measurements to be recorded alongside time.

The heat and timing data, as well as the shape of the time-temperature curve once the burning process is completed, are then saved on a computer. The bottom of the beam specimen, as well as its two lateral faces, were all exposed to the flames. The beam was removed from the furnace and cooled after the fire exposure interval.

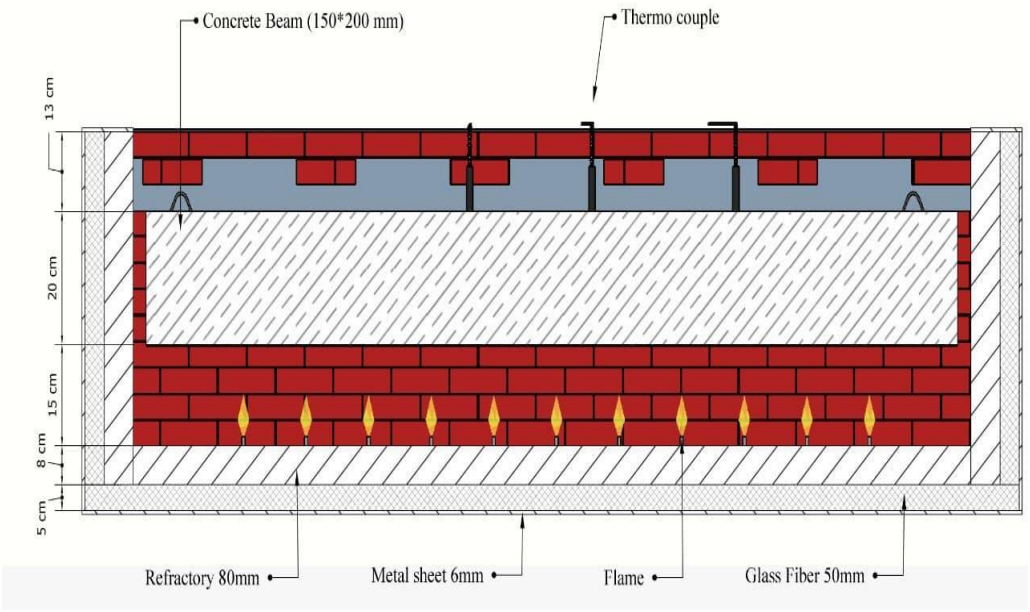

Figure 5. Configurations of burning furnace

2.4 Technique for applying jackets

After the fire and before additional strengthening, the fire-damaged beam specimens with cracked and collapsed areas were removed. Slurry-infiltrated fiber reinforced concrete (SIFCON) was used to replace the damaged portion. To simply stated, molds were filled with hooked end steel fibers in multilayers to get the desired volume fraction, the damaged LWC beams were strengthened using the strengthening approach. A specially made wooden mold was used to produce the jacket. The three-faced SIFCON jacket was cast using molds of the same form and greater size, where the mold has enough space between its surface and base concrete to enable casting of 20mm and 30mm jackets thicknesses applied at the underside and two lateral sides (U-shaped jackets), as shown in Figure (6).

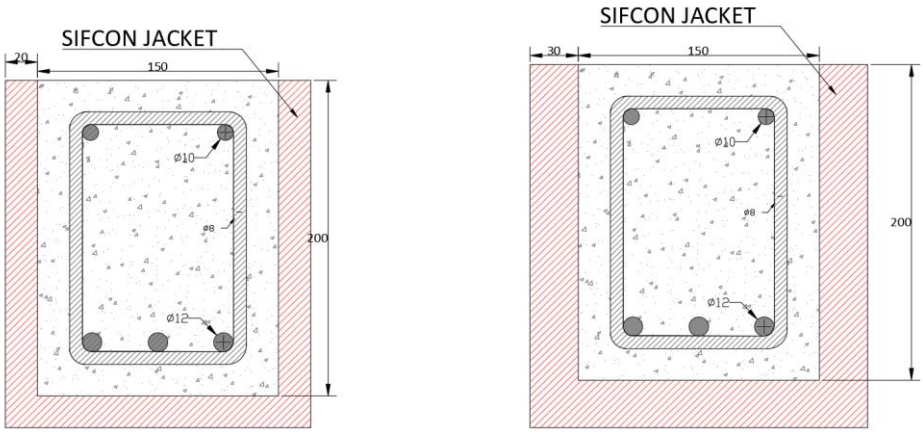

Figure 6. Strengthened section using three-faces SIFCON jacket

The previously designed slurry SIFCON mix was infiltrated into each layer. Great care was taken during the infiltration process to ensure that the fibers were evenly distributed and that no blockages formed. Figures (7) demonstrate the repairing and molding of the SIFCON jacket layers, which was performed by employing a special rubber strip as a sealant at the spot where the wooden pieces met.

The samples were then cured for another 28 days using wet burlap. The LWC beams were kept in an upside-down configuration to prevent water from reaching the original structure (lightweight concrete). The result shape shown in Figure (8).

Figure 7. The procedure of strengthening fire damaged LWC beam specimens

Figure 8. SIFCON jacket cover three faces of beam specimen

2.5 Procedures for testing

The distance between the end supports and each beam was 1.8 m. To simulate a nearly equal load on the LWC beam, a steel beam was applied and dispersed the force at two spots, separating the tested LWC beam into three sections. The distance between the two points of the load was 800 millimeters. Special supports were created from 20 mm thick hardened steel plates to sustain the applied load without deforming and to prevent crushing in the specimen body's contact point, which could alter the test findings. From one end, the supports serve as a hinge, while from the other, they serve as a roller. All beams were subjected to two-point loads using hydraulic testing equipment with a capacity of 600kN and a stroke rate of 0.02 kN/s. Until all beams were found to be

faulty, they were subjected to monotonic load tests. As indicated in Figure (9), the following measurements were acquired and saved in a data acquisition system.

Figure 9. LVDTs and Load Cell Installed on the test machine

2.6 Results of the experimental work

Each beam's configuration and exposure conditions were designated in this investigation for simplification purposes, as shown in Table (1).

Table 1. The identification of samples of concrete beam configurations and exposure scenarios

Grade	Concrete cover (mm)	Thickness of SIFCON (mm)	Beams symbol	Exposing duration (Min)
HSC LWC Beams	**20**	None	HC_1-00	0
			HC_1-01	30
			HC_1-02	60
		20	HC_1-21	30
			HC_1-22	60
		30	HC_1-31	30
			HC_1-32	60
	30	None	HC_2-00	0
			HC_2-01	30
			HC_2-02	60
		20	HC_2-21	30
			HC_2-22	60
		30	HC_2-31	30
			HC_2-32	60

The compressive strength was a well-established measurement that represented one of the main concrete engineering properties that could offer an overview of the concrete's quality. For this purpose, two batches of twelve and twelve standard cubes of (100×100×100) mm, casted using of Lightweight Expanded Clay Aggregates (LECA) as coarse aggregates were used for this experimental investigation. The first batch were tested after curing normal condition while the second were tested after exposing to 600°C fire temperature. Crushing three cubes at the ages of 7, 28, 56 and 90 days was used to determine compressive strength using a computerized testing machine with a capacity of (1900 kN) and a loading rate of (0.3 MPa/sec), and the average value of three cubes was calculated using **(BS. 1881: part 116)**. The effect of fire on the residual strength was

higher than its effect at lately ages. Generally speaking, the reduction in compressive strength for HSC at various ages ranged from 38%-46%, as can be seen in Table (2) and Figure (10).

Table 2. Test results of cube compressive strength of HS LWC samples before and after burning at 600ºC

Symbol	Age (days)	Compressive strength f_{cu} (MPa)		% Residual of compressive strength
		At 25ºC	At 600ºC	
LWHSC	7	46.60	25.02	53.7
LWHSC	28	67.33	37.13	55.2
LWHSC	56	68.12	41.69	61.2
LWHSC	90	70.21	43.74	62.3

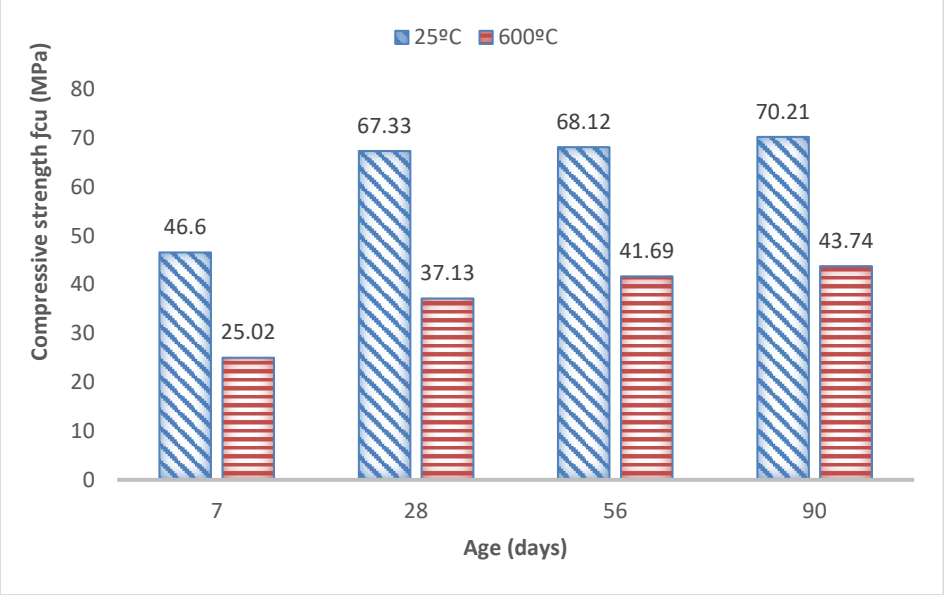

Figure 10. Concrete residual strength at various ages

Furthermore, fourteen beam specimens of HSC lightweight concrete were tested as part of the experimental program. Table 1 shows the results of the beams tests, which include the first crack load, ultimate load, residual ultimate load, and load deflection (3). The first indicator is the crack pattern, which is generated by the fracture developing in time with the applied force.

For HSLWC, the reference beam, and fire damage without strengthening specimens, very small flexural cracks with short extents appeared first within the pure bending zone (near mid span). Both the reference and damaged specimens revealed the same crack pattern as the load increased. Flexural cracks formed in both the reference and damaged specimens when the stress was increased, and already existing cracks (in the damaged specimen) expanded.

The results listed in Table (3) showing that first crack appeared at the mid-span area, with cracking loads of (17.2-25.4) and (7.5-8.8) kN, for the reference and damaged specimens, respectively. The reduced cracking load of the heat-damaged specimens might be attributable to reinforcing steel being affected. The strengthening damaged beams showed increasing in first crack load by (2.9-3.3 times) and (3.2-5.2 times) for 20mm and 30mm jacket thickness respectively comparing with reference specimen. In addition, its showed enhancement in ultimate load by (5-18%) and (28-50%) for 20mm and 30mm jacket thickness respectively.

Table 3. Results of experimental test of first crack load, ultimate load and maximum deflection for HSC LWA beam specimens exposed to fire flame

Grade	Specimen Identification	Frist Crack Load (kN)	Ultimate Load (kN)	Percentage residual Ultimate Load %	Max Deflection(mm)		
					At Mid-span	Under loading point on hinge side.	Under loading point on roller side.
HSC	HC1-00	25.4	139	100	24.87	22.41	21.05
	HC1-01	11.2	95.44	68.7	19.09	16.89	16.25
	HC1-02	8.8	81.23	58.44	20.31	18.65	15.39
	HC1-21	63.7	159.70	114.89	13.69	13.00	11.91
	HC1-22	83.1	146.40	105.3	12.19	10.79	10.59
	HC1-31	85.3	190.60	137.1	12.93	11.84	9.57
	HC1-32	80.3	178.40	128.4	13.84	12.21	12.62
	HC2-00	17.2	124.08	100	24.73	22.09	21.68
	HC2-01	11.68	89.70	72.3	28.04	25.48	20.39
	HC2-02	7.5	79.88	64.4	21.04	19.25	17.21
	HC2-21	72.3	159.90	128.9	14.63	13.09	11.13
	HC2-22	50.2	146.50	118.1	12.83	10.88	10.38
	HC2-31	98	197.20	159	14.67	12.44	12.04
	HC2-32	89.6	186.00	149.9	13.59	12.23	11.96

In all test samples, the first crack appeared about 10 cm to the left of the loading applying point at the end of the bending zone, followed by a series of tiny short cracks to the left of the first crack heading vertically, and later diagonal cracks formed and spread along the distance between the supporting and loading points. Figure (11) demonstrates that after burning, the inclination angle of diagonal fractures increases, the cracks extension shortens, and the number of cracks decreases.

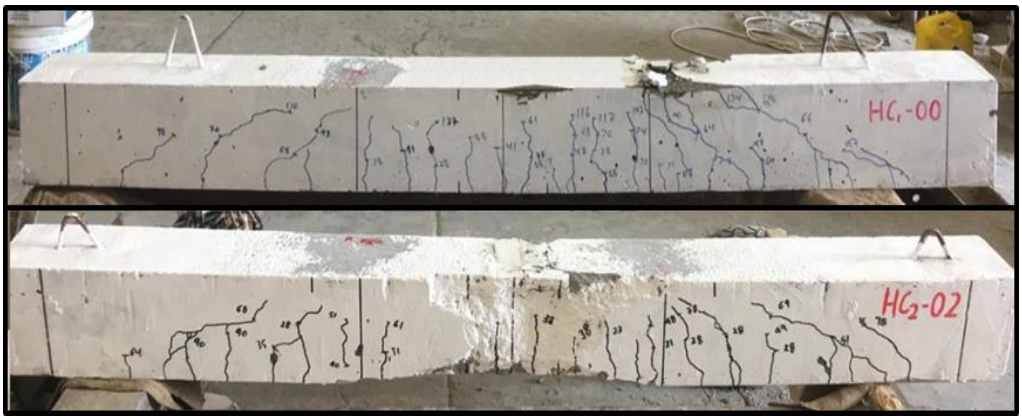

Figure 11. Pattern of cracks in HSC LWC beams before and after burning

3. Shear Strength Predicting of SIFCON-Strengthened RC LWC Beams.

Table (4) compares the predicted shear strength from the abovementioned model to the achieved shear strength of the reinforced beams tested in this study. From the results, its noticed that the shear strength reduced after burning of HSLWC beams, that the reduction was (13.9 and 13.6%) for concrete cover 20mm and 30mm respectively.

On the other hand, it is noted that the reinforcement with SIFCON jackets reflects a clear improvement in the shear strength of the beams affected by burning, with rates ranging between (45-48%) and (67.5-72%).

Table 3: A comparison of the predicted and achieved shear strength of SIFCON Jacket-strengthened beams.

Concrete cover	specimens	Expected				Achieved
		$V_{concrete}$	V_{steel}	V_{SIFCON}	V_u	V_u
20mm	HC1-00	35.9	44.6	-------	**60.37**	69.50
	HC1-02	28.08	41.2	------	51.96	40.62
	HC1-22	28.08	41.2	33.17	76.83	73.20
	HC1-32	28.08	41.2	49.76	89.28	89.20
30mm	HC2-00	33.83	42.0	------	**56.87**	50.00
	HC2-02	26.47	39.0	-------	49.10	32.20
	HC2-22	26.47	39.0	29.47	71.20	59.05
	HC2-32	26.47	39.0	44.21	82.26	74.95

4. Numerical modeling

The performance of RC structures at high temperatures is quite complex. Mechanical, physical, and thermal characteristics of concrete and steel reinforcement alter dramatically as temperature rises. In this investigation of RC structures subjected to high temperatures or fire, a computational approach [25, 26 and 27] were used extensively. Building codes [28] normally give a variant of equation for calculating fire ratings of structures when studying the effects of high temperatures.

Generally, to simulate any process or behavior of concrete elements, some main process should pass through while suing Abaqus, as follows:

- parts modelling: in this step, the geometrical modelling of the part's simulation can be created.
- Material property: in this step, the properties of the used concrete and steel parts are characterized and assigned.
- Assembly: to assemble and collect all parts involved in the simulation process.
- Step: to define type of analysis, duration of the simulation process, and solver configuration.
- Constrain and interaction: to specify type and nature of the interacted surfaced, in addition to specifying the properties of the interface.
- Loading and boundary conditions: to assign the type loading (mechanical, thermal, electrical …etc.), and boundary condition states of the samples.
- Predefined field: to define the initial status of the assembly in terms of stress, temperature distribution, … etc.
- Job: to perform and start simulation process.

The previous steps shall be detailed in next subsections. The simulation works shall be divided into three phases or stages, they are; Phase A for the reference undamaged models, Phase B for the fire damaged models, and finally Phase C for the strengthened models, as shall be presented in next subsections.

4.1. FEA Modelling of reference concrete beam samples

In this section, the stage of samples' modelling and simulation stages shall be detailed and discussed. In general, the process includes three main phases, are:

- Phase A: modelling and simulating the reference samples (unfired beam, without enhancement)
- Phase B: modelling and simulating the concrete beam samples subjected to high temperatures, and without SFCON jacket enhancement.
- Phase C: modelling and simulating the fired concrete beam after enhancing with SFCON jacketing.

4.1.1. Geometrical modelling

Abaqus provide a flexible platform for modelling in addition to its ability to import parts from other software, such like AutoCAD, with suitable and various file extensions. Generally, the procedure followed for geometrical modelling was to create parts individually according to their types, 3D, 2D, or 1D part.

Both concrete beam and jacket, 3D deformable parts were used using the extraction procedure, which in brief, the cross section of the beam or the jacket area drawn in XY plane, then a suitable extraction length are assigned to each part. On the other side, the modeling of steel reinforcement, which included longitudinal bars in addition to the ties, were modelled as one-dimensional parts, using 1D wire procedure. Although accurate simulation methodology requires identical modelling compared to the experimental program, some modifications were suggested by the previous authors which included to model steel bars as a wire element (1D part) for simplification and reduce required time to complete the analysis.

4.1.2. Materials models and assigned section

Abaqus provide various materials properties that reflects their behavior under different simulation conditions. Moreover, different failure theories are provided for metals, soils, concrete, …etc. for simulate concrete elements, it is commonly used to define two phases are elastic and plastic phases.

The elastic phase for isotropic materials is commonly characterized by two parameters are modulus of elasticity and Poisson's ratio. There are two models used characterize concrete plastic phase are concrete damaged plasticity model CDP, concrete smeared cracks model. Most of researchers recommended to use CDP model to characterize the plastic phase of quasi-brittle materials such like concrete because of its efficiency to predict concrete response under various conditions, such like monolithic and repeated loadings, plain and reinforced concrete, and application those depend on materials loading rate.

The most import aspect of such model is the ability to predict the isotropic elasticity and the isotropic tensile and compressive damaged plasticity to represent the inelastic part. Below are the properties of each plastic phase model of concrete provided by Abaqus library:

The concrete damaged plasticity model parameters in Abaqus

There are five main parameters required to be defined for The CDP model; they are, angle of dilation, eccentricity, surface plasticity flow number, viscosity, and ratio of biaxial compressive strength to the uniaxial compressive strength. these parameters are necessary to define failure surface envelope in three dimensions. Besides, the compressive (the inelastic compressive strength with plastic strain curve) and tensile behavior (inelastic stress with cracking strain curve, beyond the cracking strength) are required to be input, as can be seen in Figure (12) and Table (5) illustrates the parameters of the CDP failure surface.

Table 5. Concrete CDP material parameter selection

Parameter	**Selected value**
Material model	CDP model
E, MPa	Varied according to f'c
Possion's ratio	0.18
Dilation angel	35
*Ecc	0.1
*Fb0/fc0	1.16
*K	0.667
*Viscosity parameter	0.0001

*As recommended by Abaqus manual

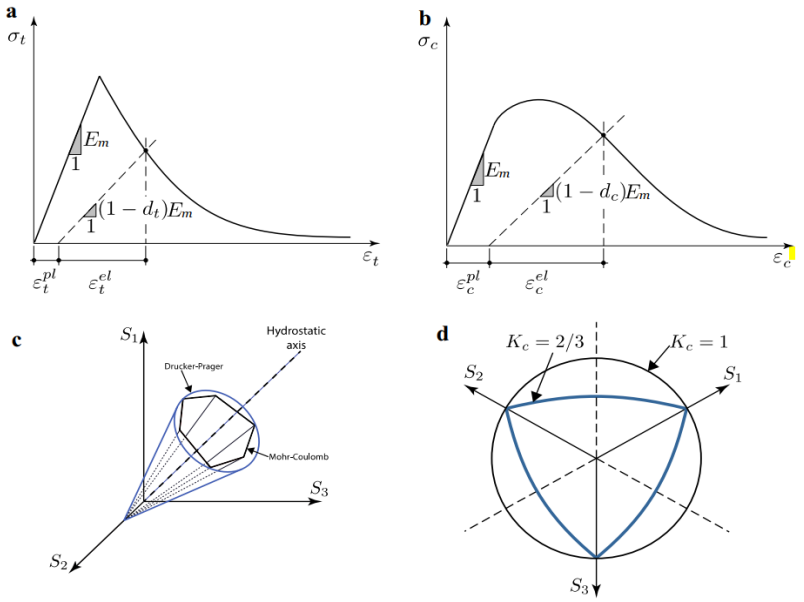

Figure 12. Tensile and compressive stress strain relation (a,b), failure surface criteria of CDP model in 3D space around the hydrostatic axis and in the deviatoric plane (c,d)

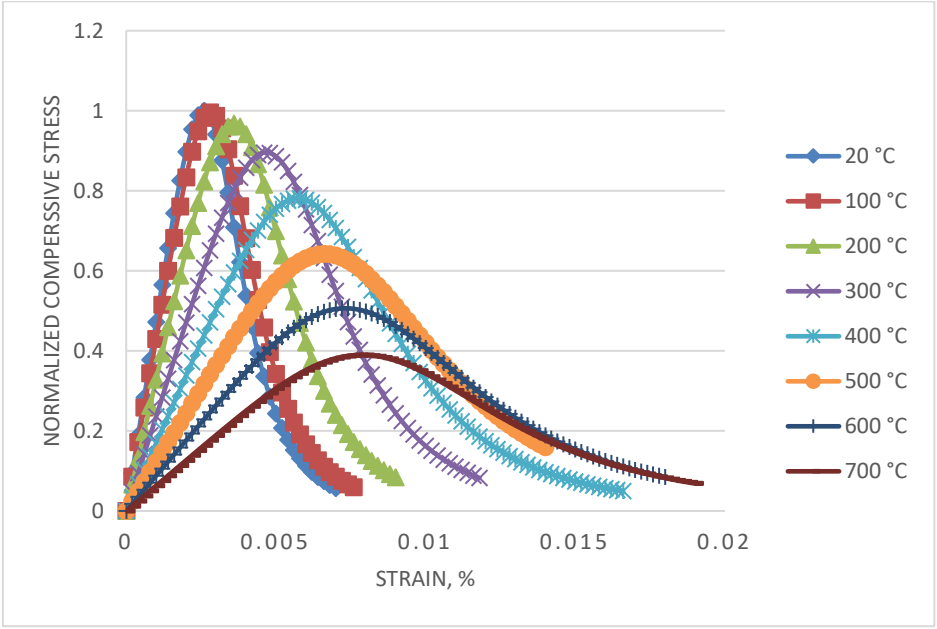

Figure 13. Normalized concrete stress – strain behavior under elevated temperatures

Another two important curves required to be input to the CDP model are the uniaxial unconfined stress-strain behavior under both compressive and tensile loading at ambient temperature (20C). These curves are segmented to elastic part, which is defined by the modulus of elasticity and passion's ratio, and the plastic part, which is defined the CDP model. The plastic phase is defined for both tensile and compressive behavior of concrete. the adopted curves are detailed in next subsections in the phase C.

Figure (14) illustrates the stress strain behavior of SFCON mixture when subjected to monolithic, uniaxial compressive and tensile stress. It can be noted that, the high percentage of steel fiber resulted a mixture with high ductility and higher sustain to resist loading, and the strain corresponded to the maximum stress approaches 0.008. it is worth mentioning that maximum compressive and tensile strength were about 94.5 MPa and 13.75 MPa, respectively.

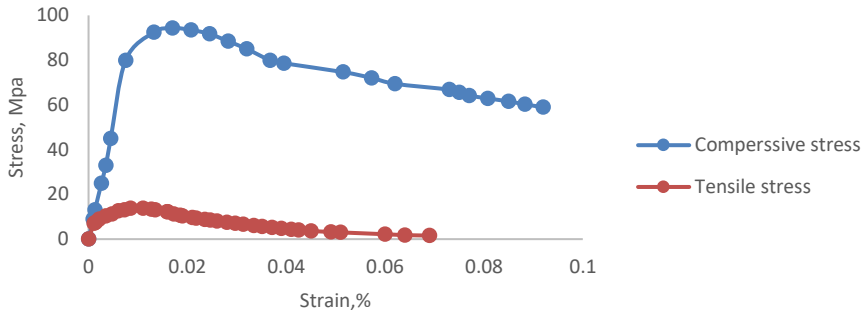

Figure 14. SICON stress- strain behavior under unconfined, uniaxial compression loading

Defining steel material behavior

For steel material, generally, there are four stress strain models which are used to characterize its behavior are engineering stress-strain, true or logarithmic stress-strain relation, elastic perfect plastic behavior, or the bilinear elastoplastic with hardening. for steel reinforcement rebars, the elastic perfect plastic behavior has been adopted herein this study. such behavior requires to define the elastic and plastic model with a minimum one point at yielding, which corresponded to a zero-plastic strain. On the other side, the linear hardening of the plastic phase requires two points as a minimum, the yield point, and the rapture point. Other mentioned relations require to define more than two points in the plastic behavior. Due to the lack of data availability for the plastic phase, the elastic perfect plastic behavior as shown in table (6), has been adopted herein this study.

Table 6. the elastic perfect plastic behavior model

Parameter	Selected value
Model type	Idealized stress strain behavior
E, MPa	200000 (ambient temperature)
Possons ratio	0.3
Yield stress, Fy	Varies according to the bar type and temperature

As a general procedure in Abaqus, each material requires a section to be defined. For instance, concrete beam part should be defined as a solid homogenous one. On the other hand, steel reinforcement sections can be defined using both beam and truss section. Beam section commonly used for one dimensional element with have regular or irregular section and requires section orientation. While truss section has equal stiffness in all direction (Circular cross section only), which is matches the steel reinforcement rebars. In this study, since there are three different bars diameter, three truss sections should be defined. Figure (15) illustrates the adopted procedure. Finally, after defining sections, each section must be assigned to tis specified part to complete materials characterization process.

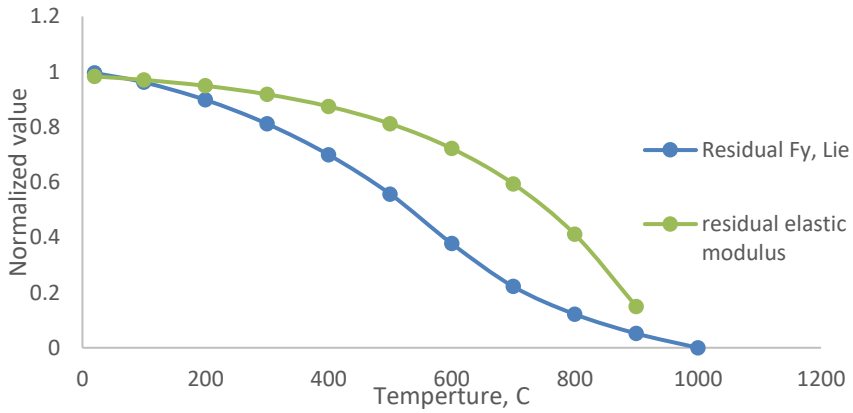

Figure 15. normalized values of the residual Fy and E values for steel bars subjected to high temperatures

4.1.3 Assembling parts

Assembling means collecting the created parts into the simulation environment using assembly module. The inserted parts then called instances. In this module, instances are created, translated, rotated, or duplicated according to the required simulation. See Figure 16.

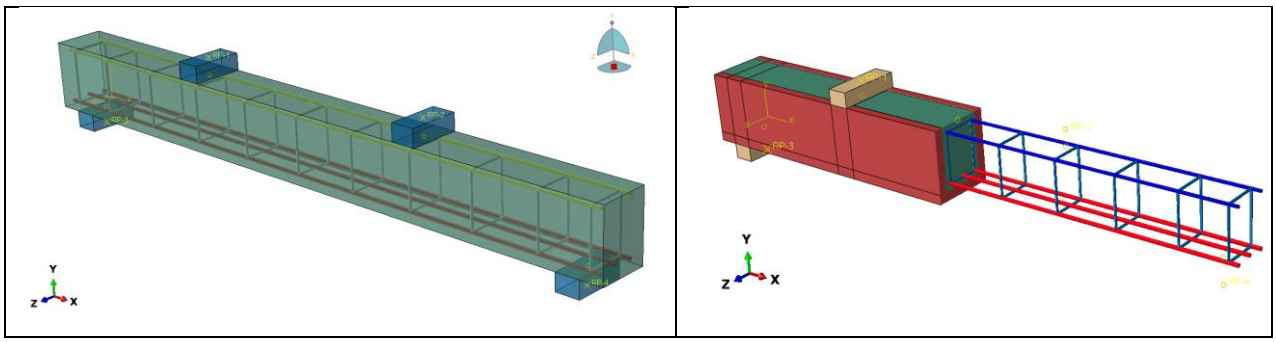

Figure 16. part assembling of the reference and strengthened models with SICON jacket

4.1.4 Meshing properties

Meshing technique is the method of segmenting and converting the simulated parts into smaller using different shapes and division algorithms. The produced parts then called (elements). In general, different types of elements are provided in Abaqus library, as can be seen in Figure (17). Continuum solid element was used for 3D parts (plates, concrete beam, SFCON jacket), 3D stress family, brick (hexagonal) shape (C3D8R). while one dimensional element (truss) family was used for steel bar reinforcement

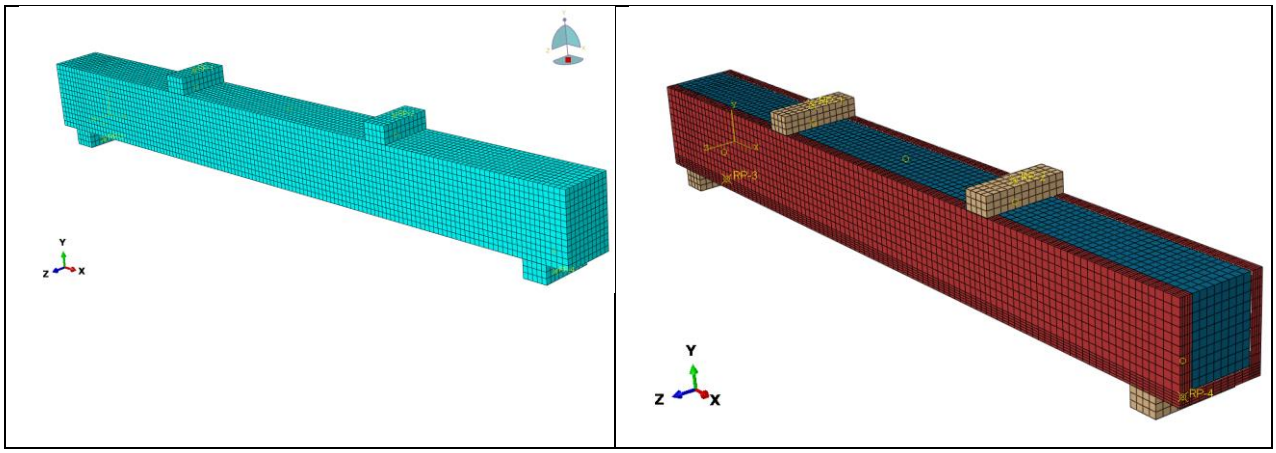

Figure 17. Meshing of the reference and the strengthened models with SIFCON jacket

5. FEM Results

5.1. Validation results of HSC at ambient temperatures (25°C)

Simulation results of the high strength concrete specimens before firing are presented herein this subsection. As can be seen in Figure (18 and 20), the load-displacement curves of the experimental and numerical approaches are close to each other for normal concrete specimen. The FEM result curve possessed higher initial stiffness than the experimental results. Also, the FEM result reflected higher load carrying capacity than the experimental results by about 7%, and corresponded displacement difference of about 1.7%. such difference can be accepted, and the adopted parameters can be said to be accurate herein this study. the von mises stress distribution for the concrete beam body and steel reinforcement, in addition to the true strain are illustrated in Figures (19 and 21).

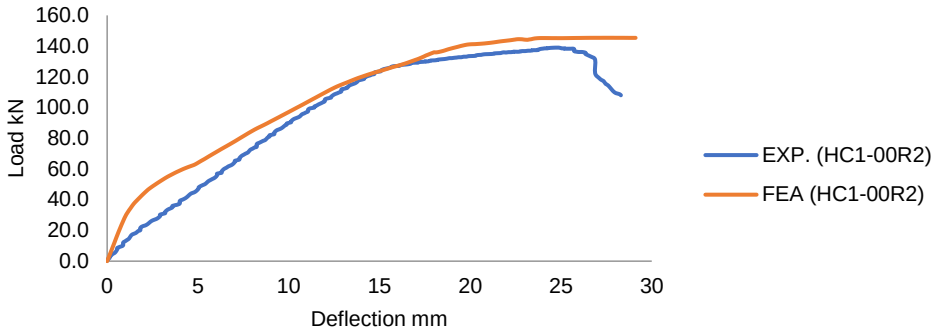

Figure 18. Load-displacement curves comparison between the FEM and the experimental work results for HC1-00

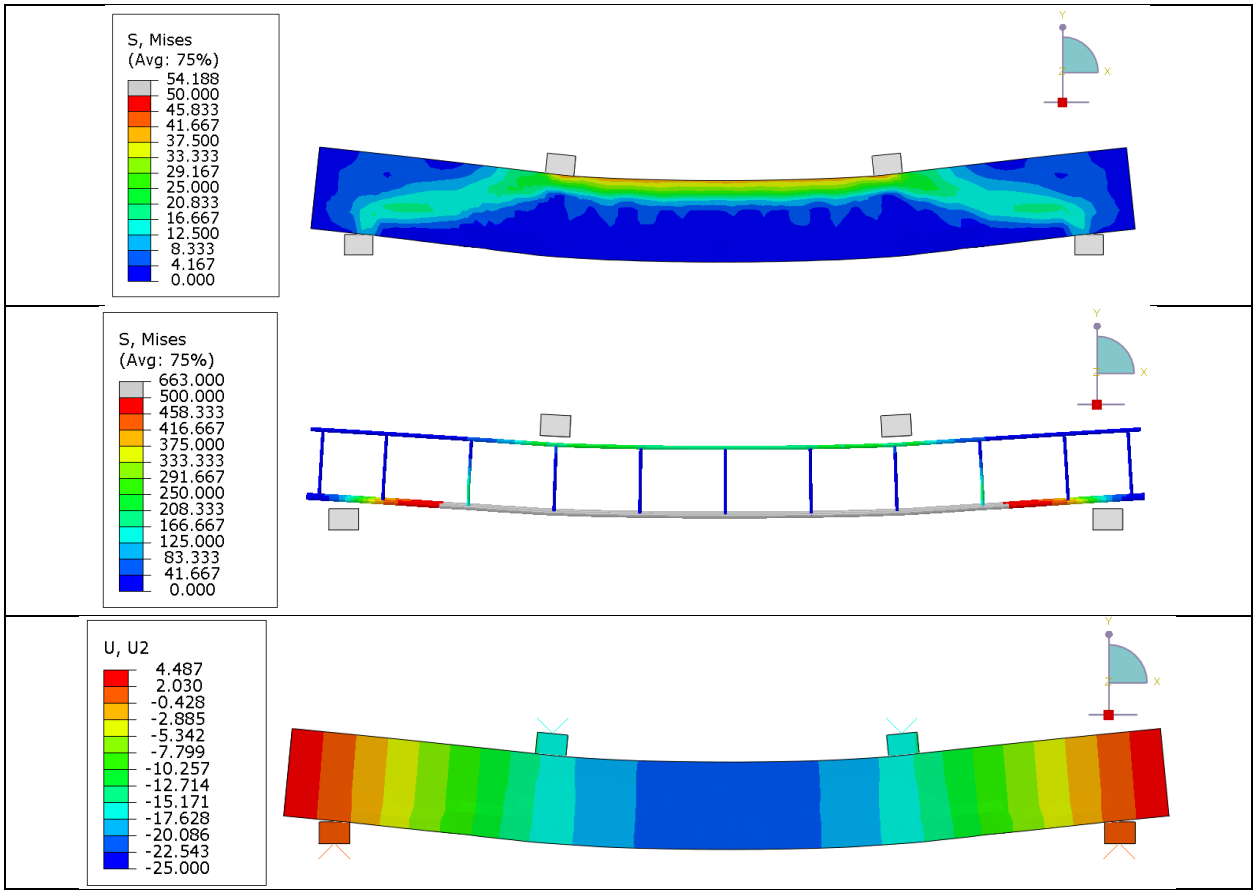

Figure 19. Von mises stress for the beam and steel reinforcement, and deflection of HC1-00

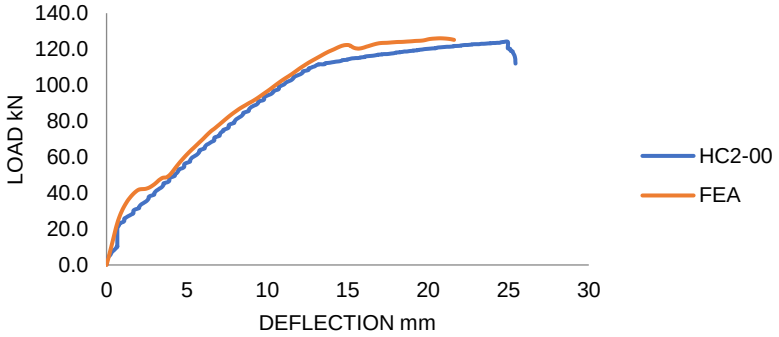

Figure 20. Load-displacement curves' comparison between the FEM and the experimental work results for HC2-00

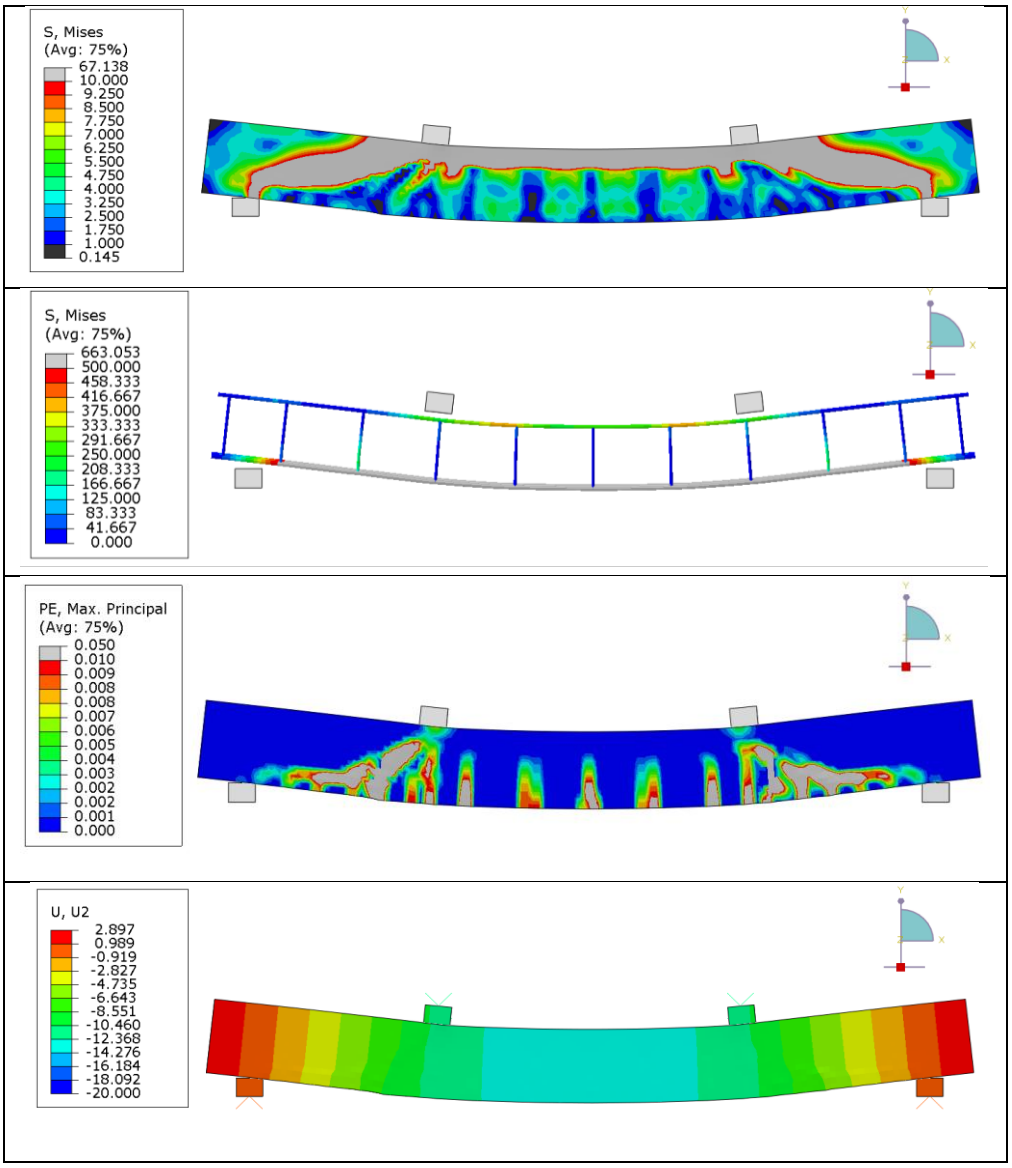

Figure 21. Von mises stress for the beam and steel reinforcement, plastic strain, and deflection of HC1-00 at the maximum load capacity

5.2. Validation results of time- temperature distribution along the beam cross section and simulation results

The heat transfer analysis of a LECA beam sample has shown very close results to those data extracted from the experimental work. As can be seen in Figure (22), and after applying TC1 amplitude curve as heating boundary to the beam surfaces, the nodal temperature parameter at the bottom steel position have shown very close result after 1 hour of heating compared to the experimental data (at TC2 location), which was approximately about 2%. while a small vibration was observed after half of an hour heating for the same location, which was about less than 10%. Moreover, there was an observable gap between the experimental and the numerical curves ranged from 10 min to 30 min. after 30 min of heating, the curves are gradually become very close to each other. In the contrary to the temperature curve at the mid of the concrete beam location (TC3), where, approximately the numerical behavior matches the experimental one most of heating time.

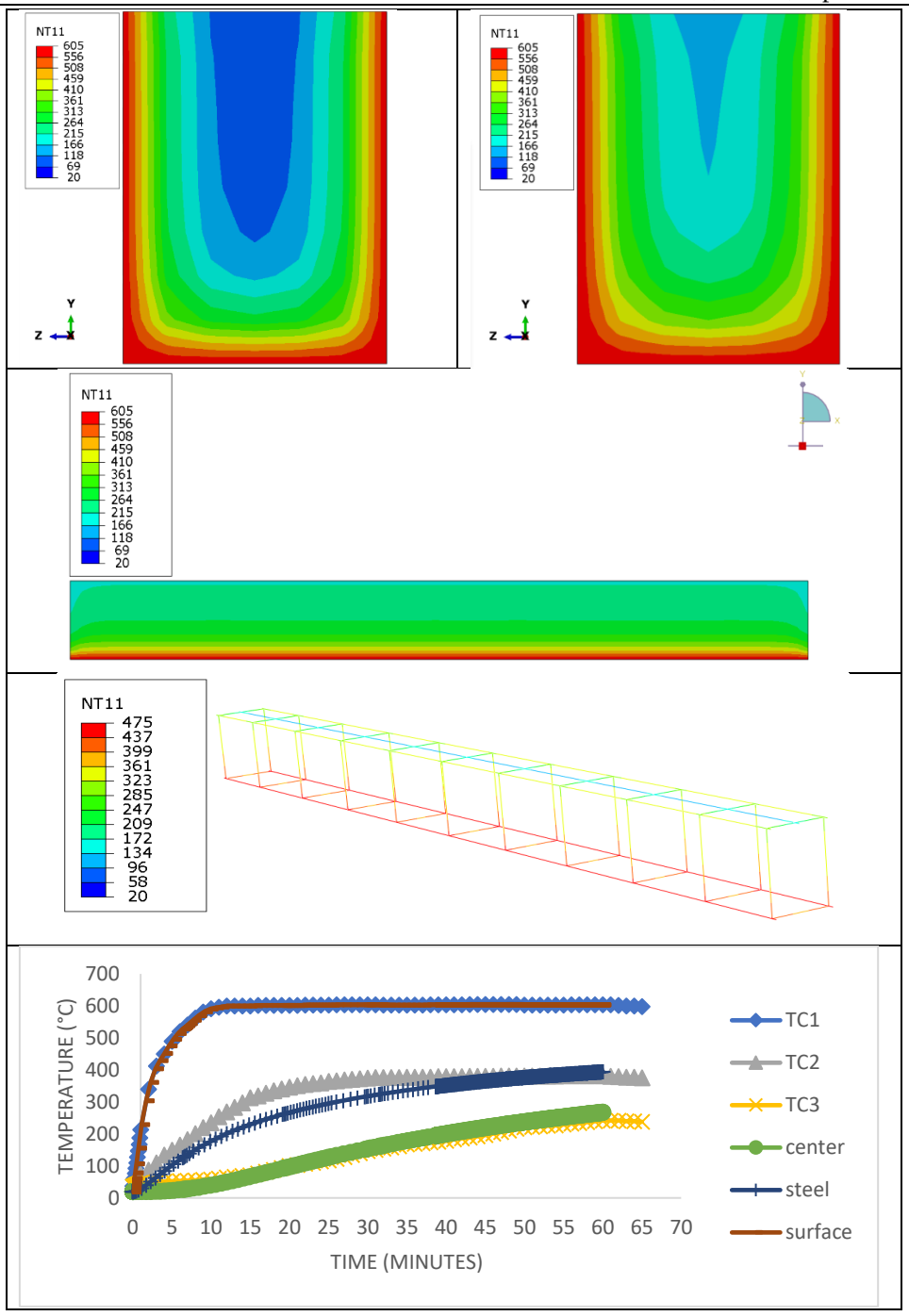

Figure 22. time- temperature distribution along the beam cross section

5.3. FEM Results of HSC beams at elevated temperatures

5.3.1. High strength concrete cover 20 mm- 1 Hour fire

Load- displacement curves result for both experimental and numerical processes for HC1-02 specimens are shown in Figure (23). The percentage of error between the FEM and the experimental results for the peak load and corresponded downward displacement were about 6.78% and 10.97%, respectively. In addition, it can be observed that both curves were matched to each other till 15 mm displacement. moreover, the degradation phase of the FEM process was higher than of the experimental result's curve. Figures (24) illustrate von mises distribution contour map stress, plastic strain, von mises of steel bars, and downward displacement distribution contour maps.

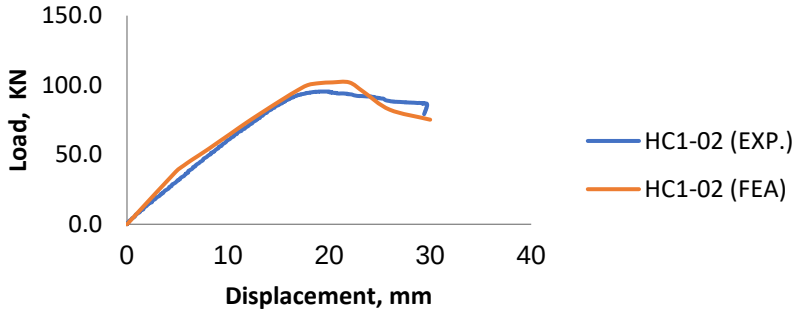

Figure 23. Comparison between load-mid span deflection curves of the FEM and the experimental work for HC1-02

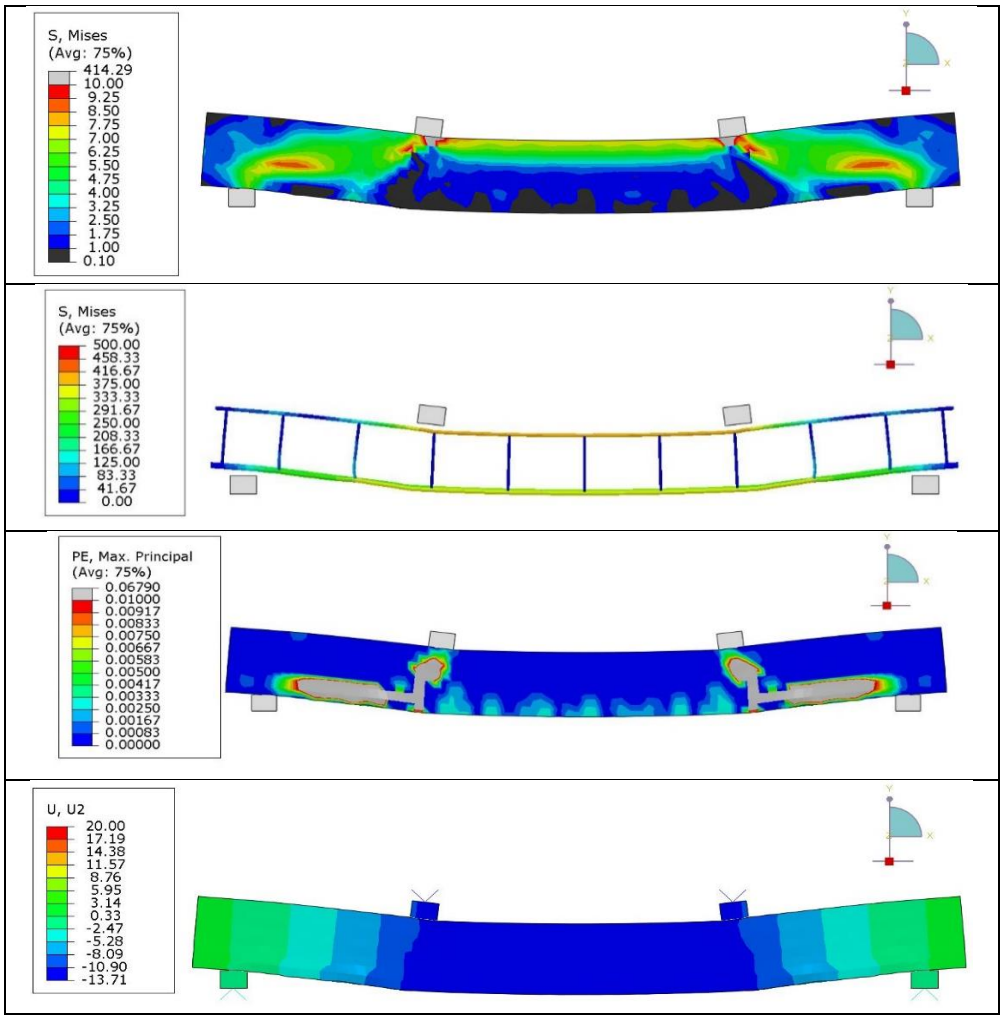

Figure 24. Von mises stress for the beam and steel reinforcement, plastic strain and deflection of HC1-02 at the maximum load capacity

Figure (25) illustrates the measured Load carrying capacity verses the midspan deflection of HC2-02 specimen based on the numerical and the experimental results. Form the previous Figure, it can be observed a good agreement have noticed when compared both mentioned curves results. The elastic stage of the FEA result was approximately matching the experimental curve in the first phase. While a smooth transition in FEM curve was observed in the contrary to the FEM one. This is because of tension stiffening parameter. In addition, it is clear the midspan displacement corresponded the maximum load capacity was somewhat varied. Overall, the percentage of error between the experimental and numerical results for the load capacity and midspan displacement were about 1.85% and 9.41%, respectively. Figure (26) illustrates von mises distribution contour map stress, plastic strain, von mises of steel bars, and downward displacement distribution contour maps.

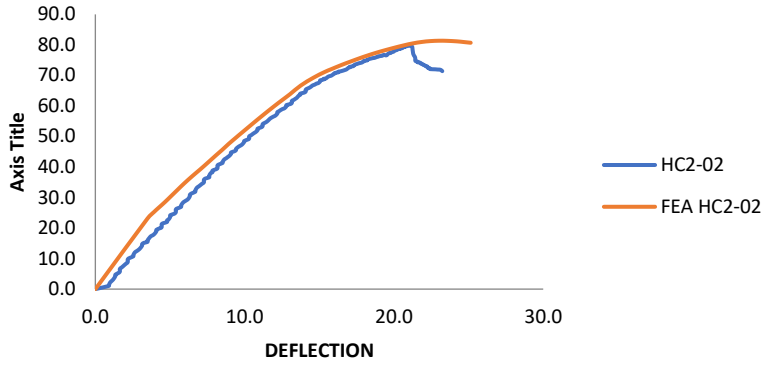

Figure 25. Comparison between load-mid span deflection curves of the FEM and the experimental work for HC2-02

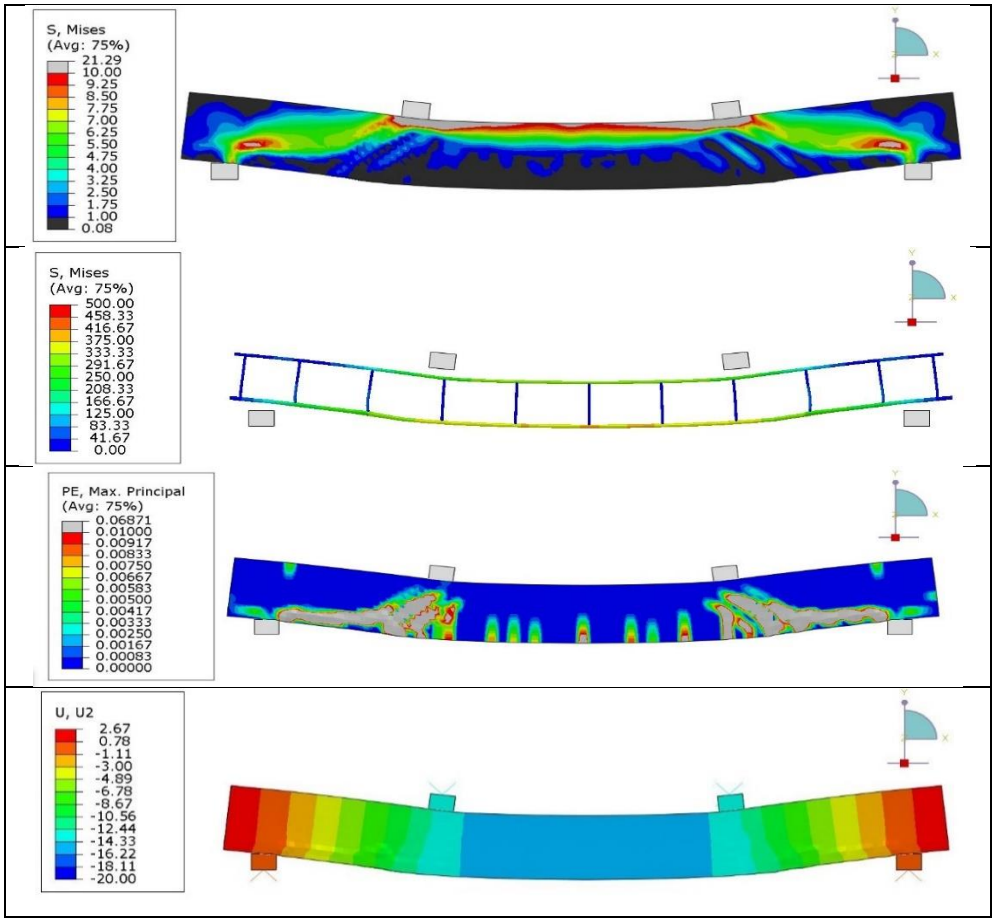

Figure 26. Von mises stress for the beam and steel reinforcement, plastic strain and deflection of HC2-02 at the maximum load capacity

5.4. validation results of postfire treated HSC beams with SFCON jacket

Figure (27) illustrates the measured Load carrying capacity verses the midspan deflection of HC1-22 specimen based on the numerical and the experimental results. The first phase matches the experimental results up to 4.1 mm displacement. after such limit, the FEM curve load was noticeably higher the load values of the experimental result. Up to the maximum load carrying capacity, a slight difference between the experimental and FEM result of the load and corresponded displacement of about 5.06% and 6.76%, respectively. followed that point, the FEM degradation behavior curve style matches the experimental curve behavior. Figure (28) illustrates von mises distribution contour map stress, plastic strain, von mises of steel bars, and downward displacement distribution contour maps.

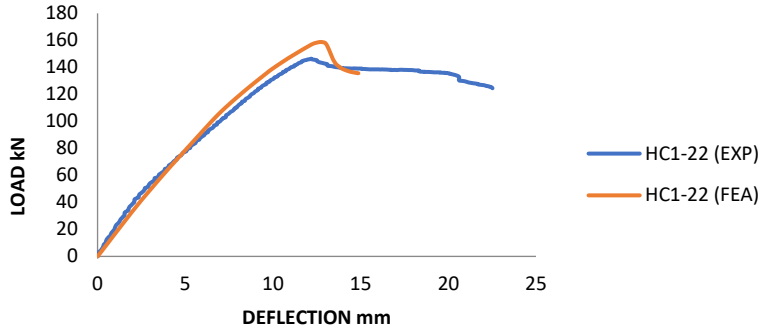

Figure 27. Comparison between load-mid span deflection curves of the FEM and the experimental work for HC1-22

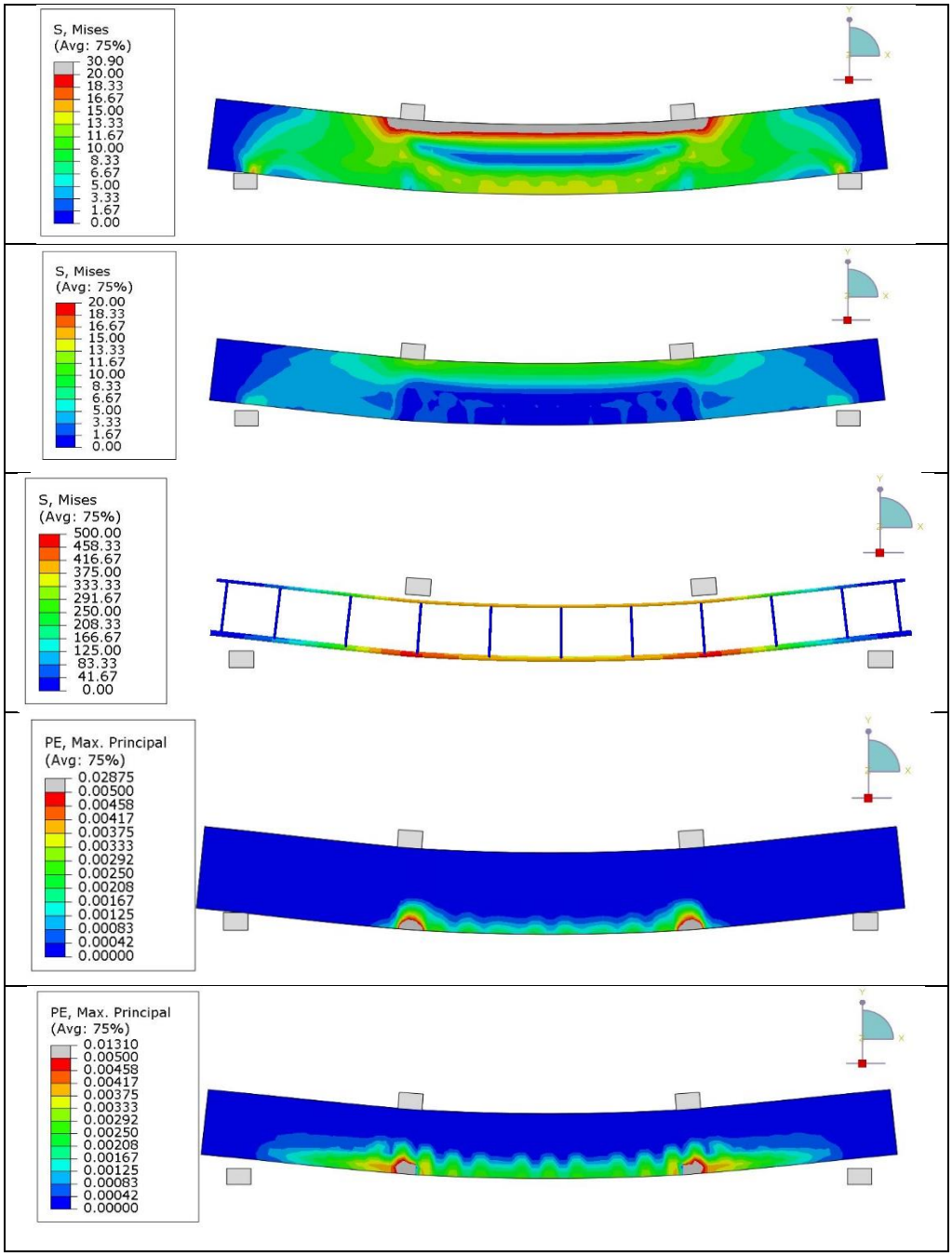

Figure 28. Von mises stress for the beam and SIFCON, Von mises stress of steel reinforcement, plastic strain for the beam for SIFCON and the beam HC1-22 at the maximum load capacity

Figure (29) clarifies an overall comparison between the experimental and numerical results of HC1-32 beam. Both were matched from the start up to 3 mm displacement. after such limit the FEA curve showed higher load resistance when compared with the experimental curve. While the displacement corresponded to the maximum load capacity of the FEM was lower than the value of the experimental results. Overall, percentage of difference between the maximum load capacity and corresponded midspan downward displacement were about 13.87% and 11.37%, respectively.

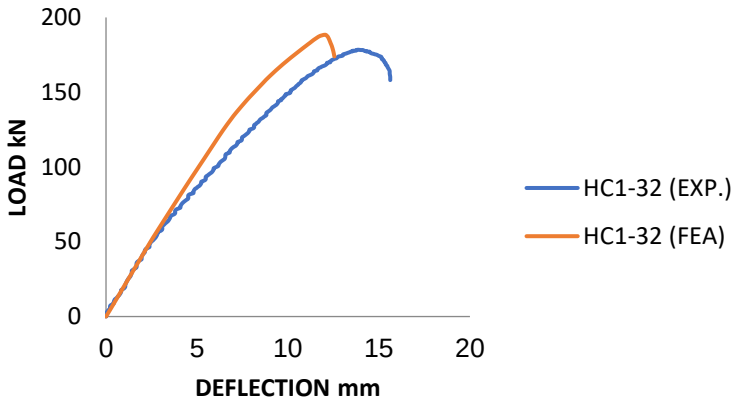

Figure 29. Comparison between load-mid span deflection curves of the FEM and the experimental work for HC1-32

Figure (30) illustrates von mises distribution contour map stress, plastic strain, von mises of steel bars, and downward displacement distribution contour maps.

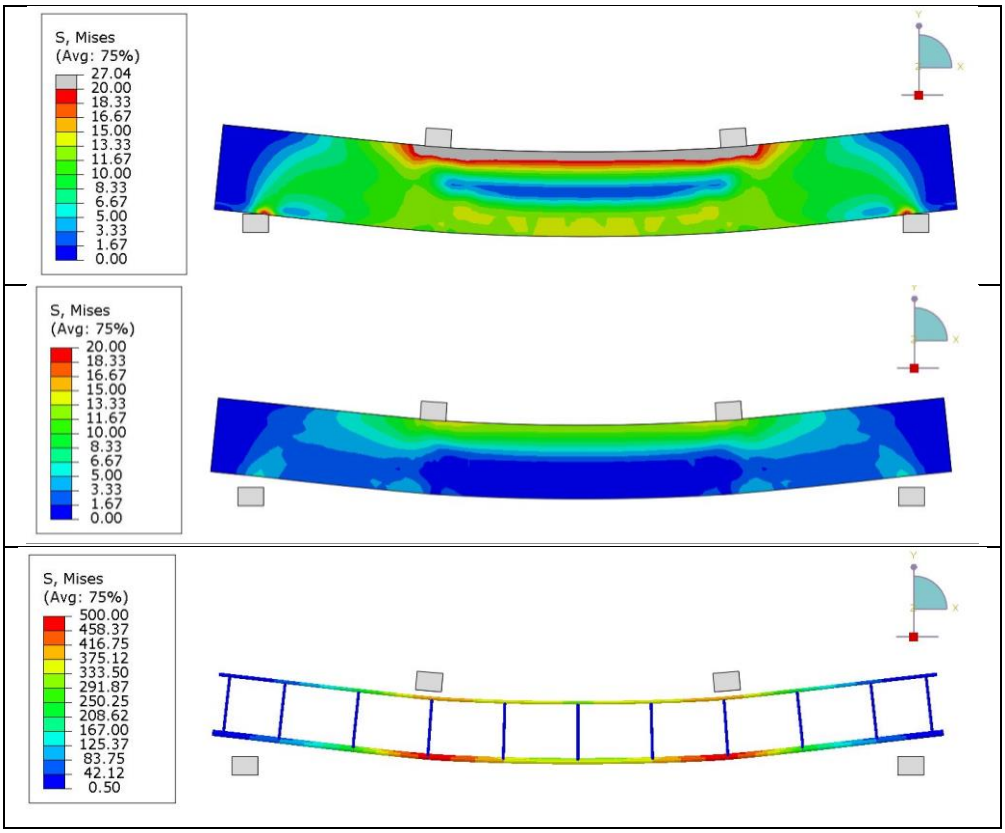

Figure 30. Von mises stress for the beam and SIFCON, Von mises stress of steel reinforcement of HC1-32 at the maximum load capacity

Figure (31) illustrates the measured Load carrying capacity verses the midspan deflection of HC2-22 specimen based on the numerical and the experimental results. The first phase matches the experimental results up to 12 mm displacement, or at the maximum load capacity. after such limit, the FEM curve load was noticeably higher

than the load value of the experimental result. A slight difference between the experimental and FEM result of the load and corresponded displacement of about 4.83% and 6.07%, respectively. followed that point, the FEM degradation behavior curve mode dropped suddenly, unmatching the experimental curve behavior, which have noticed a smooth transition between the two phases. Figure (32) illustrates von mises distribution contour map stress, plastic strain, von mises of steel bars, and downward displacement distribution contour maps.

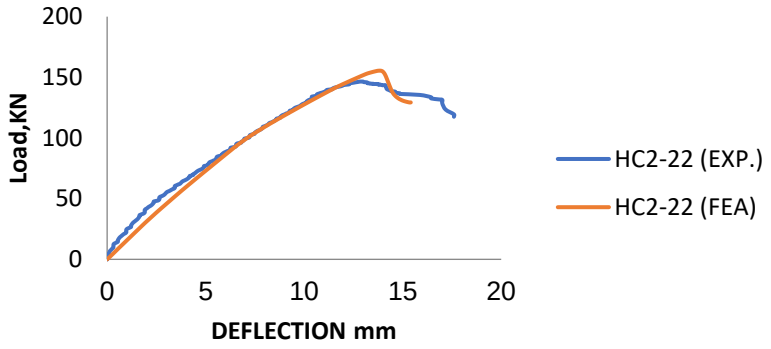

Figure 31. Comparison between load-mid span deflection curves of the FEM and the experimental work for HC2-22

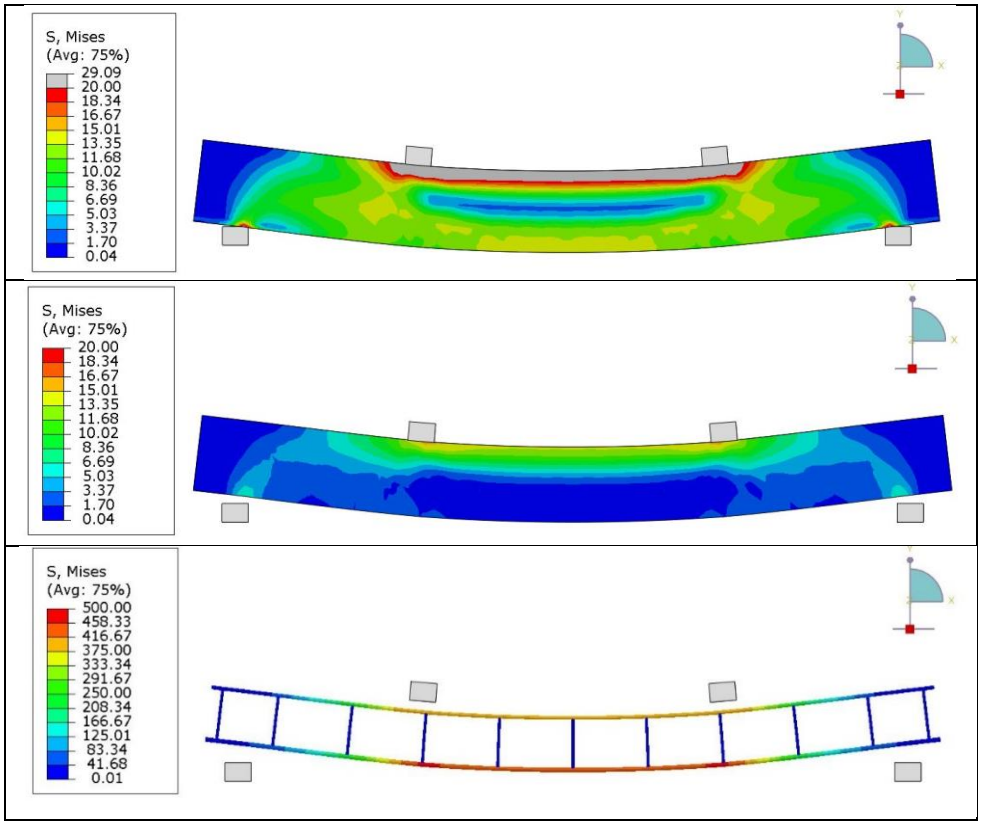

Figure 32. Von mises stress for the beam and SIFCON, Von mises stress of steel reinforcement of HC2-22 at the maximum load capacity

Figure (33) illustrates the measured Load carrying capacity verses the midspan deflection of HC2-32 specimen based on the numerical and the experimental results. The first phase matches the experimental results up to the maximum load capacity. A negligible difference between the experimental and FEM result of the load and corresponded downward midspan displacement was observed estimated of about 0.52% and 0.42%, respectively. followed that point, the FEM degradation behavior curve mode dropped suddenly, unmatching the experimental curve behavior. Also, Figure (34) illustrates von mises distribution contour map stress, plastic strain, von mises of steel bars, and downward displacement distribution contour maps.

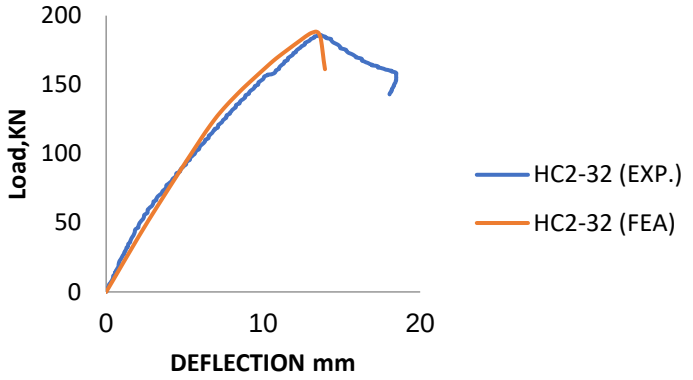

Figure 33. Comparison between load-mid span deflection curves of the FEM and the experimental work for HC2-32

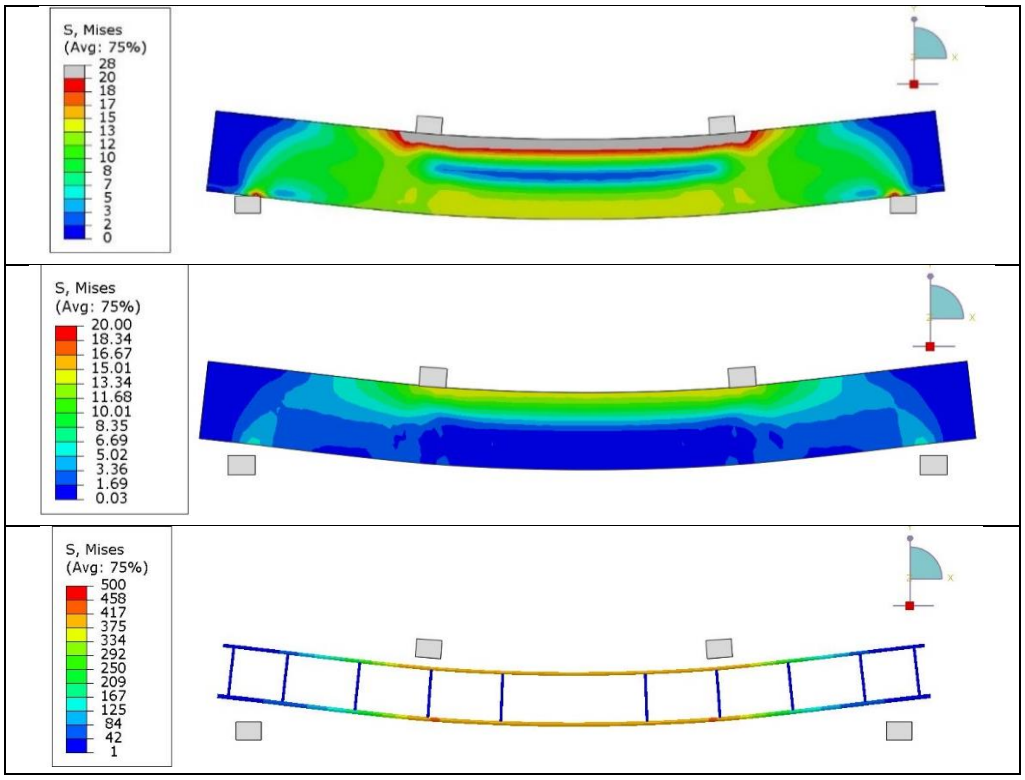

Figure 34. Von mises stress for the beam and SIFCON, Von mises stress of steel reinforcement of HC2-32 at the maximum load capacity

The mechanical and thermal properties of RC beams that have been exposed to fire are investigated using numerical simulation data that is compared to experimental results. Heat transport in RC beams is studied in two scenarios: one with a 20mm concrete cover on all three sides of the exposed beam, and the other with a 30mm concrete cover on all three sides of the exposed beam.

The temperature distribution across the beam, as well as the beam's overall structural behavior, are assessed. Specimens of high strength lightweight concrete, before and after firing, in addition to the improvement with SIFCON jacketing technique, were simulated and compared with the experimental results. For both the displacement at mid span and the maximum load carrying capacity of the specimens, the absolute error between experimental and numerical values was determined. the summery of the results is clarified in Table (7).

Table 5. summary of the results

Specimen Identification	Ultimate Load (kN) EXP.	Ultimate Load (kN) FEA	Max Deflection at Mid-span (mm). EXP.	Max Deflection at Mid-span (mm). FEA	Difference in load, %	Difference in disp., %
HC1-00	**139**	**145.17**	**24.87**	**23.56**	**4.43**	**-5.26**
HC1-01	95.44		19.09			
HC1-02	95.52	102	19.95	22.14	6.78	10.97
HC1-21	159.70		13.69			
HC1-22	146.40	153.81	12.19	13.015	5.06	6.76
HC1-31	190.60		12.93			
HC1-32	178.40	185.31	13.84	12.266	13.87	-11.37
HC2-00	**124.08**	**125.22**	**24.73**	**22.93**	**0.918**	**-7.27**
HC2-01	89.70		28.04			
HC2-02	79.88	81.36	21.04	23.02	1.85	9.41
HC2-21	159.90		14.63			
HC2-22	146.50	153.59	12.83	13.61	4.83	6.079
HC2-31	197.20		14.67			
HC2-32	186.00	186.97	13.59	13.648	0.521	0.42

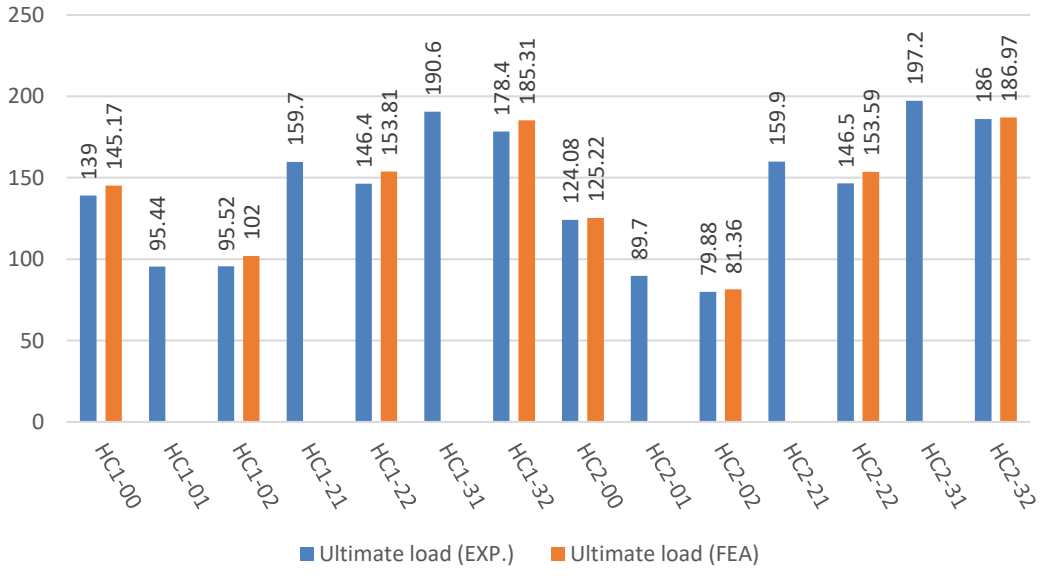

Figure 35. Comparison between the experimental and numerical results of HSC beams ultimate load

This paper proposes a viable numerical model for predicting the stiffness and strength deterioration of an RC beam at high temperatures. As a result, the aim of developing a numerical model that reflects the real behavior of RC beams when exposed to fire was accomplished, both from a material and structural stand point. This model might be used to examine and predict the behavior of lightweight reinforced concrete beam, making it a useful tool for incorporating improvements in future RC fire design regulations and methodologies.

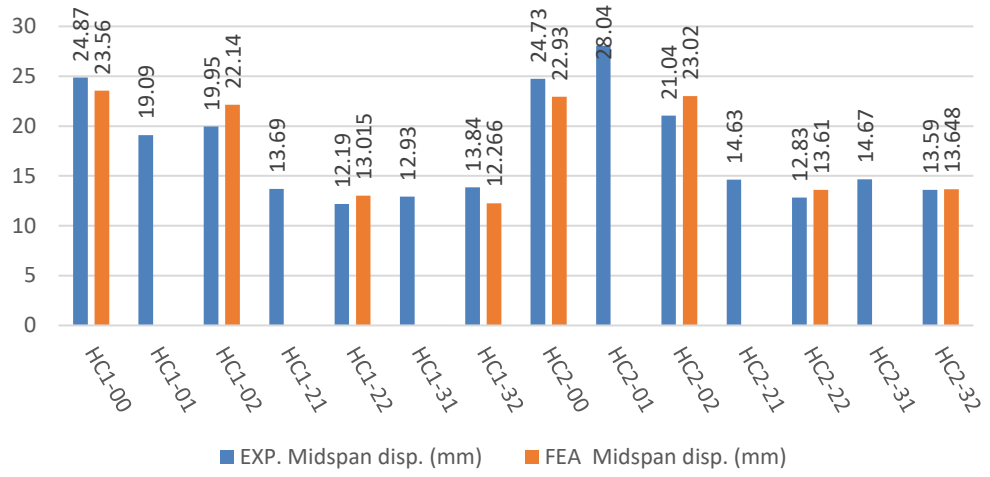

Figure 36. Comparison between the experimental and numerical results of HSC beams mid-span displacement

6. Conclusion

Accordingly, the following conclusions were drawn:

1. The application of a 20mm and 30mm SIFCON jacket on a lightweight reinforced beam increases the ultimate load capacity by (53 to 83%) and (87 to 133%), respectively, referring to a fire damaged beam. These findings demonstrate the efficiency of the suggested strategy in enhancing bearing capacity in situations of strengthening.
2. The experimentally obtained load-displacement curves are found to be in good agreement with FEM data. The lightweight beam residual strength was compared and analyzed in this work, which depicts structural damage caused by fire exposure.
3. The reinforcement with 20mm and 30mm thickness SIFCON jackets reflects a good improvement in the shear strength of the beams affected by burning, with rates ranging between (45-48%) and (67.5-72%) respectively.
4. The suggested strengthening method provides a good structural improvement at the serviceability limit phase; the mid-span deflection significantly decreased due to the significantly increased beam stiffness under service load. Where the reduction for 20mm and 30mm jacket thickness were about 39% and 36% respectively, comparing with fire damaged model.
5. The numerical validation of the obtained experimental data of load carrying capacity of the reference, fire damaged beam, and detailed temperature distribution using the ABAQUS program demonstrated a high degree of simulation process accuracy.
6. Through using of the finite element modelling with Abaqus software, the absolute error was determined between the experimental and numerical results, the results showed that the minimum and maximum determined absolute error for specimens' load carrying capacity was about 0.521% and 15.61%, respectively. on the other side, minimum and maximum determined absolute error for specimens' displacement corresponded to the max load were 0.42% and 11.42%, respectively. Since the estimated errors less than 15%, it can be said that the performed simulation process was accurate and successful when compared with other researchers' studies.
7. it can be seen that the minimum and maximum determined absolute error for specimens' load carrying capacity was about 0.521% and 15.61%, respectively. on the other side, minimum and maximum determined absolute error for specimens' displacement corresponded to the max load were 0.42% and 11.42%, respectively. accordingly, and since the estimated errors less than 15%, it can be said that the performed simulation process was accurate and successful when compared with other researchers' studies.

Declaration of competing interest

The authors declare that they have no known financial or non-financial competing interests in any material discussed in this paper.

Funding information

No funding was received from any financial organization to conduct this research.

References

[1] ACI 216.1,"Code requirements for determining fire resistance of concrete and masonry construction assemblies," Detroit: American Concrete Institute,2007.

[2] AS 3600,"Concrete structures," Sydney: Standards Association of Australia, 2009.

[3] V. R.Kodur, and N.Raut, "Performance of concrete structures under fire hazard: emerging trends,"The Indian Concrete Journal, vol.84,no.2,pp23-31,2010.

[4] A. H.Buchanan, and A. K. Abu, " Structural design for fire safety," John Wiley & Sons,2017.

[5] J.A.Purkiss,and L.Li, "Fire safety engineering design of structures," London,New York, 2013.

[6] ASTM E119–08b,"Standard test methods for fire tests of building construction and materials," ASTM International, Pennsylvania, USA, 2008.

[7] EN, 1992–1–2: "design of concrete structures. Part 1–2: general rules—structural fire design," Eurocode 2, European Committee for Standardization, Brussels, Belgium, 2004.

[8] ISO 834–1,"Fire resistance tests --- elements of building construction. Part 1: general requirement,"Geneva: International Organization for Standardization,1999.

[9] BS 476–20,"Fire tests on building materials and structures. Part 20: methods for determination of the fire resistance of elements of construction (general principles)," Milton Keynes: British Standards Institute,1987.

[10] L. Alarcon-Ruiz, G. Platret, E. Massieu, and A. Ehrlacher, “The use of thermal analysis in assessing the effect of temperature on a cement paste,” Cem. Concr. Res., vol. 35, no. 3, pp. 609–613, 2005, doi: 10.1016/j.cemconres.2004.06.015.

[11] R. H. Haddad and L. G. Shannis, “Post-fire behavior of bond between high strength pozzolanic concrete and reinforcing steel,” Constr. Build. Mater., vol. 18, no. 6, pp. 425–435, 2004, doi: 10.1016/j.conbuildmat.2004.03.006.

[12] R. Kodur, “Fire Performance of HSC and NSC,” pp. 1–4, 1999, [Online]. Available: http://www.nrc.ca/irc.

[13] C. Beyler, J. Beitel, N. Iwankiw, B. Lattimer, I. Hughes Asociattes, and N. F. P. Association, “Fire resistance testing for performance-based fire design of buildings,” p. 150, 2007, [Online]. Available: http://www.nfpa.org/research/fire-protection-research-foundation/reports-and-proceedings/building-and-life-safety/fire-resistance.

[14] F. Fingerloos,“Fédération internationale du béton – FIB. fib Bulletin 38,” Fire Des. Concr. Struct. - Mater. Struct. Model., vol. 102, p. 106, 2007.

[15] The Institution of Structural Engineers,“Guide to the Advanced Fire Safety Engineering of Structures,”London: Institution of Structural Engineers,2007.

[16] S. Bratina, I. Planinc, M. Saje, and G. Turk, “Non-linear fire-resistance analysis of reinforced concrete beams,” Struct. Eng. Mech., vol. 16, no. 6, pp. 695–712, 2003, doi: 10.12989/sem.2003.16.6.695.

[17] S. Bratina, M. Saje, and I. Planinc, “The effects of different strain contributions on the response of RC beams in fire,” Eng. Struct., vol. 29, no. 3, pp. 418–430, 2007, doi: 10.1016/j.engstruct.2006.05.008.

[18] D. Di Capua and A. R. Mari, “Nonlinear analysis of reinforced concrete cross-sections exposed to fire,” Fire Saf. J., vol. 42, no. 2, pp. 139–149, 2007, doi: 10.1016/j.firesaf.2006.08.009.

[19] V. K. R. Kodur and M. Dwaikat, “A numerical model for predicting the fire resistance of reinforced concrete beams,” Cem. Concr. Compos., vol. 30, no. 5, pp. 431–443, 2008, doi: 10.1016/j.cemconcomp.2007.08.012.

[20] V. Kodur, M. Dwaikat, and N. Raut, “Macroscopic FE model for tracing the fire response of reinforced concrete structures,” Eng. Struct., vol. 31, no. 10, pp. 2368–2379, 2009, doi: 10.1016/j.engstruct.2009.05.018.

[21] S. F. El-Fitiany and M. A. Youssef, “Assessing the flexural and axial behaviour of reinforced concrete members at elevated temperatures using sectional analysis,” Fire Saf. J., vol. 44, no. 5, pp. 691–703, 2009, doi: 10.1016/j.firesaf.2009.01.005.

[22] B. Wu and J. Z. Lu, “A numerical study of the behaviour of restrained RC beams at elevated temperatures,” Fire Saf. J., vol. 44, no. 4, pp. 522–531, 2009, doi: 10.1016/j.firesaf.2008.10.006.

[23] C. Bailey, “Science and technology developments in structural fire engineering,” Struct. Eng. Int. J. Int. Assoc. Bridg. Struct. Eng., vol. 19, no. 2, pp. 155–164, 2009, doi: 10.2749/101686609788220240.

[24] ISO 834-1,"Fire Resistance Tests-Elements of Building Construction. Part 1: General Requirement,” International Organization for Standardization, Geneva, Switzerland, 1999.

[25] Z. Huang, I. W. Burgess, and R. J. Plank, "Nonlinear analysis of reinforced concrete slabs subjected to fire," Structural Journal, vol.96, no.1, pp.127-135,1999.

[26] S. Bratina, M. Saje, and I. Planinc, “The effects of different strain contributions on the response of RC beams in fire,” Eng. Struct., vol. 29, no. 3, pp. 418–430, 2007, doi: 10.1016/j.engstruct.2006.05.008.

[27] D. Di Capua and A. R. Mari, “Nonlinear analysis of reinforced concrete cross-sections exposed to fire,” Fire Saf. J., vol. 42, no. 2, pp. 139–149, 2007, doi: 10.1016/j.firesaf.2006.08.009.

[28] C. E. N.Eurocode, "2: Design of Concrete Structures—Part 1–2: General Rules—Structural Fire Design," European Standard: London, UK,2004 .